



HAL
open science

Probabilistic Structural Health Monitoring Using Passive-Only Damage Detection by Reciprocity of Green's Function Reconstructed from Diffuse Acoustic Fields

Jeffery Tippmann, Xuan Zhu, Francesco Lanza Di Scalea

► **To cite this version:**

Jeffery Tippmann, Xuan Zhu, Francesco Lanza Di Scalea. Probabilistic Structural Health Monitoring Using Passive-Only Damage Detection by Reciprocity of Green's Function Reconstructed from Diffuse Acoustic Fields. EWSHM - 7th European Workshop on Structural Health Monitoring, IFFSTTAR, Inria, Université de Nantes, Jul 2014, Nantes, France. hal-01021247

HAL Id: hal-01021247

<https://inria.hal.science/hal-01021247>

Submitted on 9 Jul 2014

HAL is a multi-disciplinary open access archive for the deposit and dissemination of scientific research documents, whether they are published or not. The documents may come from teaching and research institutions in France or abroad, or from public or private research centers.

L'archive ouverte pluridisciplinaire **HAL**, est destinée au dépôt et à la diffusion de documents scientifiques de niveau recherche, publiés ou non, émanant des établissements d'enseignement et de recherche français ou étrangers, des laboratoires publics ou privés.

PROBABILISTIC STRUCTURAL HEALTH MONITORING USING PASSIVE-ONLY DAMAGE DETECTION BY RECIPROCITY OF GREEN'S FUNCTION RECONSTRUCTED FROM DIFFUSE ACOUSTIC FIELDS.

Jeffery Tippmann¹, Xuan Zhu¹, Francesco Lanza di Scalea¹

¹ Structural Engineering, University of California, San Diego, La Jolla, CA

Contact email: jtippman@ucsd.edu

ABSTRACT

A new passive damage detection approach is proposed using the reciprocity of the Green's function. This is achieved using a known method to reconstruct the forward and backward time-domain Green's functions between any two detection points in an acoustic diffuse field from the ensemble average of their cross-correlation functions. Damage is detected when the similarity between the forward and backward signals decreases due to the wave nonlinearities introduced by the discontinuity. Proof-of-principle results are discussed for an aluminum plate. A simulated diffuse field was created on the structures using a grid of independent random excitations. Aiming at damage detection, the observations were collected by two sets of experiments considering pristine structure and the case with simulated damages. Due to the lack of exact knowledge to the statistical distribution (most likely in a real world wind turbine blade), a bootstrapping parameter estimation was proposed in this study. To classify the cases with and without damages, a feature study was conducted based on multiple bootstrapping results. This damage detection method combining with the empirical statistical framework can be appropriately extended to any structure with significant acoustic or ultrasonic noise sources.

KEYWORDS : *Diffuse field, Reciprocity, Green's function, PC, ambient noise*

INTRODUCTION

The use of ambient noise induced structural vibrations for non-destructive evaluation (NDE) and structural health monitoring (SHM) has become a particular attractive field of research [1-4]. Wind turbines are particularly attractive structure because of the wind, aerodynamic, and machinery noise sources [5]. When these natural excitations are used instead of active excitations, the complexity of a deployed system decreases substantially by using passive only sensors and data systems that listening to the structure during operation. The data collected can be the processed using a number of methods. This paper presents a new approach to disseminating the data recorded.

A promising method applied to SHM uses the reconstruction of the structural impulse response function from passive-only measurements [1, 3]. The same benefits of a traditional active pitch catch inspection are realized with the availability of the impulse response recovered passively. Because a forward and backwards impulse response function is generated for any sensor pair, an array of sensors provides many different impulse response functions available for interpretation.

To extend this approach into new applications the Green's functions estimations were obtained by a bootstrapping of spatial and segmented time signals. A feature study was conducted to quantify the presence of nonlinearity. Multiple features and damage indexes were extracted to compare the differences between the estimations of forward and backward Green's function. A set of univariate and multivariate analysis were performed to provide suggestions for feature selection for further studies.

1 BACKGROUND

1.1 Passive reconstruction of Green's function

The impulse response function can be reconstructed using a collection of noise sources because of the known understanding that the Green's function emerges through the cross correlations in diffuse fields [6]. In order to experimentally reconstruct the Green's functions, the diffuse field is created from a collection of random excitations on the structure. The cross correlation function, $C_{ij,k}(t)$, for each k th spatially varying excitation location, is expressed in equation (1)

$$C_{ij,k}(t) = \int_0^T s(\tau)_{i,k} * s(t + \tau)_{j,k} d\tau \quad (1)$$

where t is time, T is the observation period, τ is the cross correlation time lag $s_{i,k}$ is the signal measured by sensor (i) for k th excitation, and $s_{j,k}$ is the signal measured by sensor (j) for the k th excitation.

The time derivative of the ensemble average of the cross correlation functions, denoted by the $\langle \rangle$ operator, is used to recover the estimates of the forward ($G_{ji}(t)$) and backward ($G_{ij}(-t)$) Green's functions. The two functions correspond to the causal and anticausal portions of the cross correlation function, as expressed in equation (2) with the positive (t) and negative time ($-t$).

$$\frac{d\langle C_{ij} \rangle}{dt} \propto G_{ji}(t) - G_{ij}(-t) \quad (2)$$

1.2 Damage detection by reciprocity

In the presence of damage the forward and backwards Green's functions are expected to be different, owing to the break in reciprocity [7]. Therefore, for the presented method, several statistical features of the forward and backwards impulse response function are used as the features in a multivariate principal component analysis. For simplicity of equations in Table 1, the forward impulse response function is referred to as y and the backwards impulse response function is referred to as x . Note $*$ stands for cross correlation; $\| \cdot \|$ denotes the L2 norm; Max is the maximum of the signal, Ppk is the peak to peak value, and FFT is the fast fourier transform.

2 EXPERIMENTAL SETUP

The passive damage detection technique summarized in the previous section was tested on a 1.6 mm thick aluminum 5052 plate measuring 1220 mm wide by 1220 mm long, as shown in Figure 1 (a). Six, high-frequency PCB 352B accelerometers were placed in a hexagon-like pattern in the center of the plate, creating 15 unique wave paths between sensors. In this experiment, damage in the plate was simulated by adding a 25 mm wide piece of modeling clay at one location shown in Figure 1 (b). Each experiment, with and without clay, involved recording the responses in the accelerometers for 5 seconds while the shaker, generating random white noise excitation, was hand-held and moved between during random white noise excitation at all 576 locations in the 50.8 mm x 50.8 mm grid drawn on the plate. The use of clay was a convenient way to provide a proof-of-principle result on the use of the wave reciprocity metric for "damage" detection.

Table 1: Description of features studied in this paper. Each individual feature was included in the principal component analysis

Domain	Features				
Time	#1 Max ratio	$\text{Max}(y) / \text{Max}(x)$	#2 Mean ratio	$\text{Mean}(y) / \text{Mean}(x)$	
	#3 Mean square ratio	$\frac{1}{n} \sum_{i=1}^n y_i^2 / \frac{1}{n} \sum_{i=1}^n x_i^2$	#4 RMS ratio	$\sqrt{\frac{1}{n} \sum_{i=1}^n y_i^2} / \sqrt{\frac{1}{n} \sum_{i=1}^n x_i^2}$	
	#5 Standard dev. ratio	$\text{Std}(y) / \text{Std}(x)$	#6 Variance ratio	$\text{Var}(y) / \text{Var}(x)$	
	#7 Skewness ratio	$\frac{E(y-\bar{y})^3}{\sigma_y^3} / \frac{E(x-\bar{x})^3}{\sigma_x^3}$	#8 Kurtosis ratio	$\frac{E(y-\bar{y})^4}{\sigma_y^4} / \frac{E(x-\bar{x})^4}{\sigma_x^4}$	
	#9 Crest factor ratio	$\frac{\text{Max}(y)}{\text{RMS}(y)} / \frac{\text{Max}(x)}{\text{RMS}(x)}$	#10 K factor ratio	$\frac{\text{Max}(y)\text{Rms}(y)}{\text{Max}(x)\text{Rms}(x)}$	
	#11 DI reciprocity	$1 - \frac{ (y*x)_{\tau=0} }{\ y\ \ x\ }$	#12 Normal Var	$\frac{ \text{Var}(y) - \text{Var}(x) }{\sqrt{\text{Var}(y)\text{Var}(x)}}$	
	#13 Normal RMS	$\frac{ \text{RMS}(y) - \text{RMS}(x) }{\sqrt{\text{RMS}(y)\text{RMS}(x)}}$	#14 (Normal RMS) ²	$\frac{(\text{RMS}(y) - \text{RMS}(x))^2}{\text{RMS}(y)\text{RMS}(x)}$	
	#15 Normal Max	$\frac{ \text{Max}(y) - \text{Max}(x) }{\sqrt{\text{Max}(y)\text{Max}(x)}}$	#16 DI Max	$\text{Max} \left(\frac{ \text{Max}(y) }{ \text{Max}(x) }, \frac{ \text{Max}(x) }{ \text{Max}(y) } \right)$	
	#17 Normal Ppk	$\frac{ \text{Ppk}(y) - \text{Ppk}(x) }{\sqrt{\text{Ppk}(y)\text{Ppk}(x)}}$	#18 DI Ppk	$\text{Max} \left(\frac{ \text{Ppk}(y) }{ \text{Ppk}(x) }, \frac{ \text{Ppk}(x) }{ \text{Ppk}(y) } \right)$	
	Frequency	# 19 Energy, 8.0-8.5 kHz ratio	$\frac{\sqrt{\frac{1}{n} \sum_{i=8\text{kHz}}^{8.5\text{kHz}} \text{FFT}(y) ^2}}{\sqrt{\frac{1}{n} \sum_{i=8\text{kHz}}^{8.5\text{kHz}} \text{FFT}(x) ^2}}$	# 20 Energy 8.5-9.0 kHz ratio	$\frac{\sqrt{\frac{1}{n} \sum_{i=8.5\text{kHz}}^{9\text{kHz}} \text{FFT}(y) ^2}}{\sqrt{\frac{1}{n} \sum_{i=8.5\text{kHz}}^{9\text{kHz}} \text{FFT}(x) ^2}}$
		# 21 Energy 9.0-9.5 kHz ratio	$\frac{\sqrt{\frac{1}{n} \sum_{i=9\text{kHz}}^{9.5\text{kHz}} \text{FFT}(y) ^2}}{\sqrt{\frac{1}{n} \sum_{i=9\text{kHz}}^{9.5\text{kHz}} \text{FFT}(x) ^2}}$	# 22 Energy 9.5-10 kHz ratio	$\frac{\sqrt{\frac{1}{n} \sum_{i=9.5\text{kHz}}^{10\text{kHz}} \text{FFT}(y) ^2}}{\sqrt{\frac{1}{n} \sum_{i=9.5\text{kHz}}^{10\text{kHz}} \text{FFT}(x) ^2}}$
		# 23 Energy 10-10.5 kHz ratio	$\frac{\sqrt{\frac{1}{n} \sum_{i=10\text{kHz}}^{10.5\text{kHz}} \text{FFT}(y) ^2}}{\sqrt{\frac{1}{n} \sum_{i=10\text{kHz}}^{10.5\text{kHz}} \text{FFT}(x) ^2}}$		

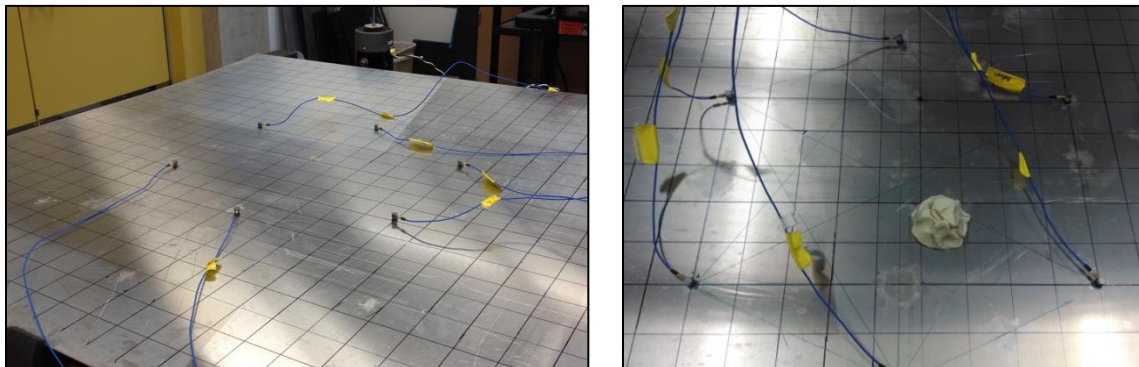


Figure 1: (a) Aluminum plate with accelerometer placement and grid of excitation locations (each gridbox is 50.8 cm x 50.8 cm) with wave path between sensors drawn. (b) Aluminum plate with modeling clay used as simulated damage

3 DATA ANALYSIS

The data recorded by the 6 sensors from two sets of experiments ('pristine' and 'damaged') at the 576 locations consist of 3456 time signals with length of 500,000. For each signal, the waveform is divided into 25 segments with no overlap. To compute the cross correlations between all possible sensor pair combinations, two raw signals of the same time segment from the specific sensor pair are analyzed and stored for the ensemble average. By randomly sampling and averaging the cross correlations from 343,000 samples out of 14,400 sample pool respectively, followed by a time differentiation, the estimations of the forward and backward Green's functions of all sensor pairs are obtained from the causal and anticausal portions of the correlation function. For each sensor pair, this bootstrapping procedure is conducted multiple times in order to build up the sample population, resulting in 100 estimations for both the forward and backward impulse response functions. To evaluate the reciprocity in both cases the statistics features (see Table 1) using the forward and backward Green's functions are computed.

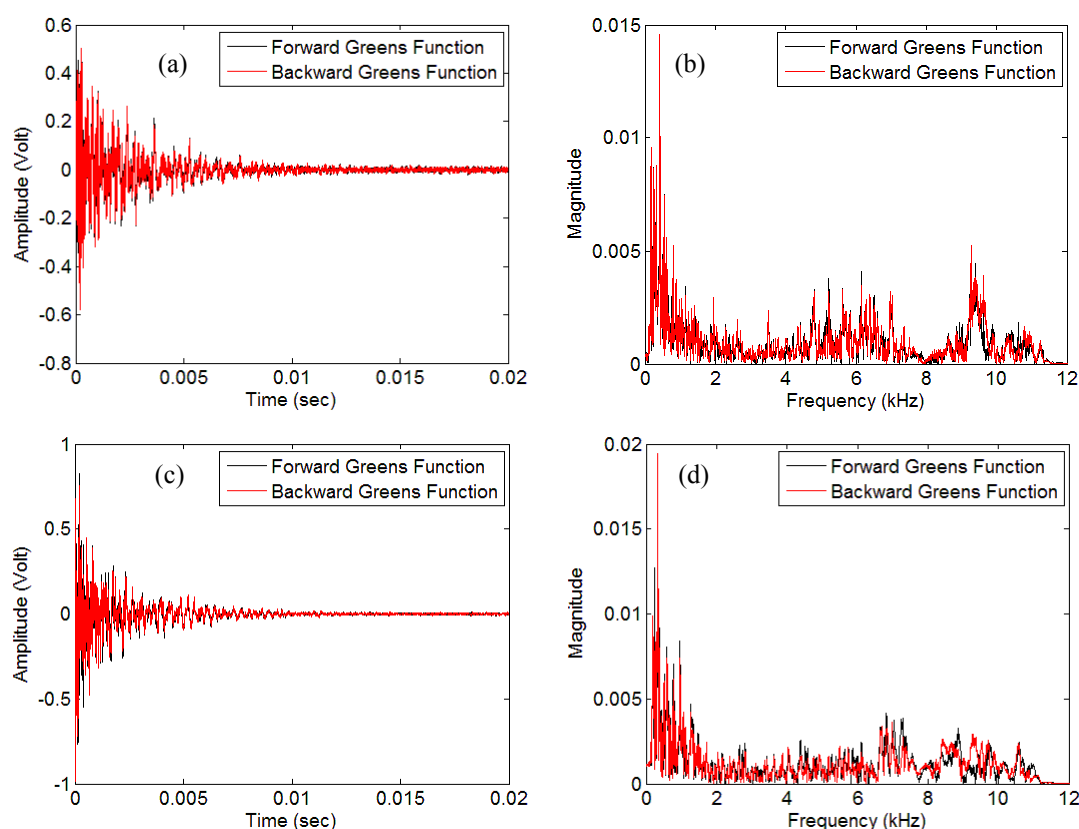


Figure 2 Estimation of the forward and backward Greens functions of sensor pair 1-5 (a) 'pristine' time signals (b) 'pristine' FFT results (c) 'damaged' time signals (d) 'damaged' FFT results

One out of the a hundred estimations of the forward and backward Green's functions from the first time segment of sensor pair 1-5 is shown in Fig.2. In Fig. 2 (a), strong correlation is observed as expected in the case of 'pristine' structure, indicating a satisfactory reciprocity; the frequency domain analysis in Fig. 2 (b) also demonstrates a good agreement across the frequency bins. On the other hand, there is deviation between the causal and anticausal portions in Fig. 2 (c) corresponding to the appearance of nonlinearity caused by the presence of clay, while the deviations in frequency ranges from 7 to 11 kHz become noticeable in Fig.2 (d).

An univariate feature analysis is first conducted to demonstrate the differences on reciprocities between ‘pristine’ and ‘damaged’ cases. By using all the distinguishable features, a Principal Component Analysis (PCA) was conducted on the feature space to visualize the projections onto the eigenvectors corresponding to dominant variations. At this stage, since the population of the forward and backward Green’s functions has been built up, the histograms of selective features from 15 sensor pairs are studied. The histograms of the selective features from sensor pair 1-5 and 3-4 are plotted in Fig. 3 and 4. In this feature analysis, the sensitivities of different sensor pairs indicate the presence of clay at the wave path or not.

For sensor pair 1-5, the clay results in significant scatter in the wave path and feature analysis shows obvious difference between the ‘pristine’ and ‘damaged’ cases as shown in Fig. 3. When it comes to sensor pair 3-4, the presence of clay does affect the diffuse filed and the wave path 3-4 has been influenced: as shown in Fig. 4 (a), the mean value ratio between the forward and backward Green’s function shifts and its variance becomes larger when the clay presents in the structure, which indicates more scattering energy led by the clay in the diffuse filed; and the other statistical characteristics of the other features have been altered by the presence of wave scatter as shown in Fig. 4 (b-d). However, it is much less distinguishable with the feature histograms overlap in two sets of data compared to sensor pair of 1-5 in Fig. 3. With the sensitivity of this univariate feature study to the presence of the clay, it suggests the potential of defect identification and localization via the selective features analysis and the sparse sensor arrays.

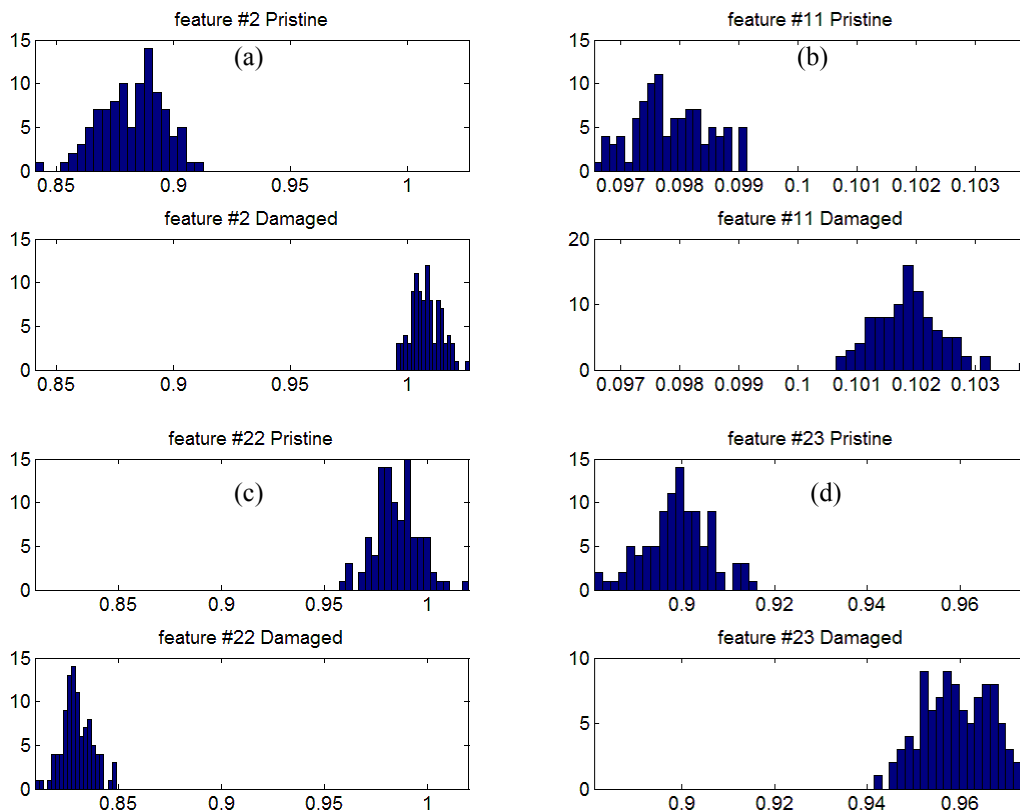


Figure 3 Selections of histogram of features from sensor pair 1-5: (a) feature #2 mean value; (b) feature #11 (c) feature #22 (d) feature #23 for both the ‘pristine’ and ‘damaged’ cases

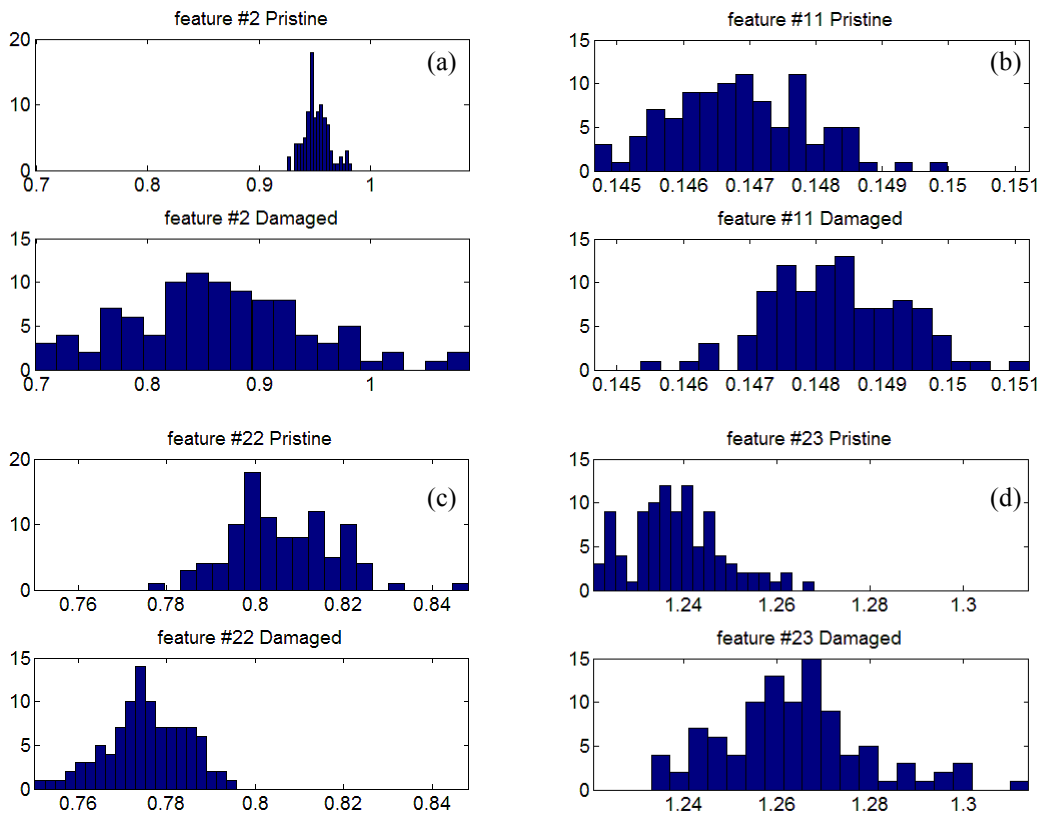


Figure 4 Selections of histogram of features from sensor pair 3-4: (a) feature #2 mean value; (b) feature #11 (c) feature #22 (d) feature #23 for both the ‘pristine’ and ‘damaged’ cases

PCA has been commonly used in machine learning for dimensionality reduction and visualization, by projecting data into a lower dimensional space through a linear transformation [8]. In the field of SHM in the past decade [9-11], researchers have applied PCA to the various feature spaces in order to visualize the data of different structural states or de-couple the structural damage effect from the environmental effect(s). With N samples of data in p dimensions, PCA projects the feature vectors into a new p dimensional vector space via a linear transformation. In this study, both the first 50 bootstrapping results from ‘pristine’ and ‘damaged’ cases are used as training data to construct the eigenvector space. The eigenvalue analysis reports that over 90% of the full data variance has been encapsulated in the first two principal components. Thus, feature vectors from all data sets are projected onto the first two eigenvectors to characterize the data in vector space. Then, the K Nearest Neighbor (KNN) search is applied to find the closest class and label the data point in the vector space. Fig. 5 illustrated the 2D visualization shows the existence of separable clusters for ‘pristine’ and ‘damaged’ cases on selective sensor pairs whose Greens functions are supposed to be significantly affected by the clay presence: the black and red points represent the data from ‘pristine’ and ‘damaged’ cases respectively; the circles and crosses stand for the training set and test set respectively. The black and red clusters show the data sets are separable in this two-dimensional projection and the test data sets overlap closely to the training set clusters for both the ‘pristine’ and ‘damaged’ cases. Furthermore, 100% of the test data are correctly assigned to their actual structural conditions within the projected vector space for the selected wave paths by using the KNN classifier.

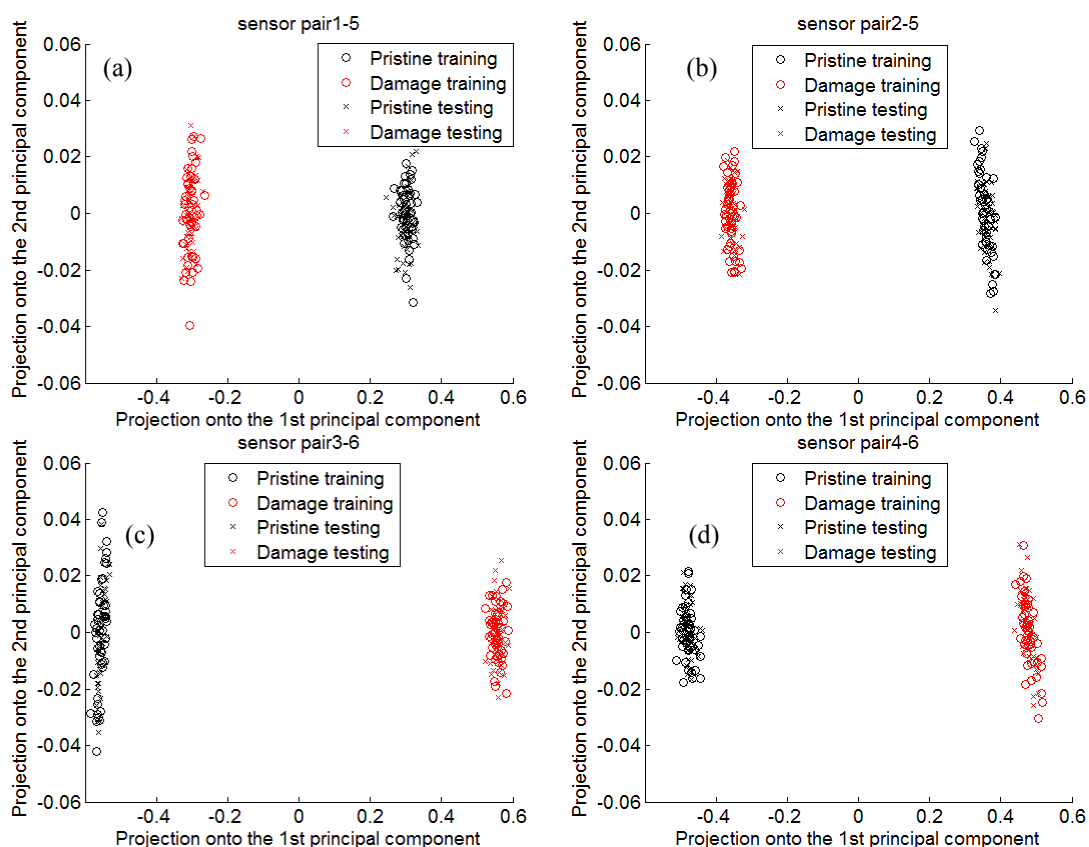


Figure 5 The feature vectors projected onto the first two principal components from sensor pair of: (a) 1-5; (b) 2-5; (c) 3-6; (d) 4-6.

The univariate and multivariate feature analysis demonstrate the two data sets are separable for selected wave paths since the feature extraction and PCA preserve the statistical characteristic of raw data sets. It also shows the potential of defect identification and localization via the selective features analysis and the sparse sensor arrays.

CONCLUSION

In this study, the time segment bootstrapping strategy was conducted by building up the population of the estimates of Green’s functions. Multiple features and damage indices were used to characterize the presence of nonlinearity introduced by simulated clay. A statistical univariate analysis was performed for feature selection based on the sensitivities to the presence of simulated damage, following with PCA to visualize the clustering of ‘pristine’ and ‘damaged’ cases for selected wave paths.

The results show a promising way to look at passively acquired data. While in this experiment the diffuse field is created through a collection of noise sources, the real world application of this method would not have noise sources from spatially known positions. In that case, the bootstrapping strategy can only happen in the time domain unless different operational conditions are considered. Because the forward and backwards impulse response functions should hold perfect reciprocity in a linear structure, the feature list is populated based on a comparison of these two functions. Because of the breakdown in reciprocity, the feature lists show potential for a passive damage detection system that utilizes a statistical analysis of the data set available.

REFERENCES

- [1] K.G. Sabra, A. Srivastava, F. Lanza di Scalea, P. Rizzo, S. Conti. Structural health monitoring by extraction of coherent guided waves from diffuse fields. *The Journal of the Acoustical Society of America*. 123(1), EL8-13, 2008
- [2] S.W. Doebling, C.R. Farrar. Computation of Structural Flexibility for Bridge Health Monitoring using Ambient Modal Data. *Proc. Of 11th ASCE Engineering Mechanics Conference. Ft. Lauderdale, Fl.* pp1114-1117, May 1996.
- [3] K.G. Sabra, S. Huston. Passive structural health monitoring of high-speed naval ship from ambient vibrations. *Journal of the Acoustical Society of America*. 129, pp 2991, 2011.
- [4] C.R. Farrar, S.W. Doebling, D.A. Nix. Vibration-based damage identification. *Philosophical Transaction of Royal Society of London A*. 369, 13-149, 2001.
- [5] S. Wagner, R. Bareiß, G. Guidati. *Noise mechanism in wind turbines*. Springer Berlin Heidelberg, pp. 67-92, 1996.
- [6] Lobkis OI and Weaver RL (2001) On the emergence of the Green's function in the correlations of a diffuse field. *The Journal of the Acoustical Society of America* 110(6): 3011-3017
- [7] Sohn H, Park HW, Law KH, and Farrar CR. Damage Detection In Composite Plates by Using an Enhanced Time Reversal Method. *Journal of Aerospace Engineering*. 20(3): 141-151.
- [8] S. Sharma. *Applied Multivariate Techniques*. John Wiley and Son, New York, 1996
- [9] H. Sohn, C. Farra, N. Hunter, K. Worden. Applying the LANL statistical pattern recognition paradigm for structural health monitoring to data from a surface-effect fast patrol boat, Los Alamos National Laboratory Report LA-13761-MS, Jan, 2001
- [10] Y. Ying. A data-driven framework for ultrasonic structural health monitoring of pipes. PhD dissertation, Carnegie Mellon University, 2012
- [11] N. Dervilis, M. Choi, S.G. Taylor, R. J. Barthorpe, G. Park, C.R. Farrar, K. Worden. On damage diagnosis for a wind turbine blade using pattern recognition. *Journal of sound and vibration*, 333(2014) 1833-1850.